Journal of Molecular Graphics and Modelling 29 (2010) 436–442

Contents lists available at ScienceDirect

Journal of Molecular Graphics and Modelling

journal homepage: www.elsevier.com/locate/JMGM

Acetylenic inhibitors of ADAM10 and ADAM17: In silico analysis of potency and selectivity

Eamonn F. Healy*, Pablo Romano, Moises Mejia, Gunnar Lindfors III

Department of Chemistry, St. Edward's University, 3001 South Congress Ave., Austin, TX 78704, USA

ARTICLE INFO

Article history:
Received 26 June 2010
Received in revised form 18 August 2010
Accepted 21 August 2010
Available online 21 September 2010

Keywords:
ADAM17
TACE
ADAM10
Metalloproteinase inhibition docking
Molecular modeling hydroxamate

ABSTRACT

The matrix metalloproteinase family has been a pharmaceutical target for most of the last three decades, but success has been hampered by unwanted side effects caused by lack of selectivity, poor oral bioavailability and decreased potency *in vivo*. The surface-expressed metalloproteinases ADAM10 and ADAM17, the latter also referred to as TACE, play important roles in various physiological processes, especially involving tissue repair and development. Because of its role in the release of the cytokine TNF-α TACE has been a key target for pharmaceutical intervention in the treatment of rheumatoid arthritis. An extensive body of structural activity data has been developed for a series of small molecule inhibitors of TACE based on a sulfonamide scaffold containing key acetylenic substituents. We have undertaken an extensive molecular modeling study of select members of this ligand group to better understand the structural nuances involved in the development of ever more potent TACE inhibitors, and identify those elements of structure-based design that would enhance the selectivity of such inhibitors for TACE over ADAM10. Results include the identification of a flexible loop, comparable to that found in other MMPs that plays a subtle, yet significant, role in determining inhibitor potency.

1. Introduction

The matrix metalloproteinases (MMPs) and the ADAMs (A Disintegrin And Metalloproteinase domains) are zinc containing proteolytic enzyme families implicated in a variety of physiological processes such as inflammation, wound healing and tissue development. The pathologies associated with either increased or decreased activities of these enzymes include, but are not limited to, conditions such as rheumatoid arthritis, diabetes, osteopenia, Alzheimer's disease and cancer. The roles of metalloproteinases in cancer are complicated by the fact that most tumor cells, and frequently the surrounding stromal cells, synthesize MMPs to facilitate invasion into surrounding connective tissue and promote metastasis.

The structural similarity between the active sites of various MMPs and ADAMs has presented a major challenge for the design of specific inhibitors. In addition to the unwanted side effects caused by lack of selectivity, other reasons for the low success rate in the development of therapeutic targets to date include poor oral bioavailability and decreased potency *in vivo*. Most of the structure-based inhibitor design thus far has focused on ligands containing a zinc-binding group (ZBG) and substituents designed to occupy the S_1'–S_3' enzyme sub-sites as shown in Fig. 1A. Whereas the zinc-binding group provides high affinity but low specificity, P_1' substituents are major determinants of both potency and selectivity. For most MMPs and ADAMs a wide range of P_2' substituents are tolerated, including rings that cyclize to P_3', and steric bulk at this position is often beneficial for oral bioavailability. A wide range of P_3' substituents are also well tolerated, and polar or charged groups at this position can affect biliary excretion.

Also called TACE, or Tumor Necrosis Factor (TNF-α) converting enzyme, ADAM17 is implicated in Rheumatoid Arthritis (RA) through the production of the pro-inflammatory cytokine TNF-α. A number of crystal structures are available from the Research Collaboratory for Structural Bioinformatics (RCSB) Protein Data Bank (PDB) for the catalytic domain of TACE co-crystallized with various ligands. As shown in Fig. 1A the binding of the peptidomimetic TAPI-2, Fig. 2A, to TACE clearly demonstrates the effectiveness of the hydroxamate ZBG. The isobutyl P_1' substituent binds in the largely hydrophobic S_1' pocket, while the bulky tert-butyl P_2' substituent sits in the shallow S_2' sub-site. The methyl P_3' substituent points towards the large S_3' cleft with the diaminoethyl group extending out from the active site. Beyond their limited selectivity inhibitors such as TAPI-2 suffer from other deficiencies common to peptidomimetics, such as poor solubility, metabolic lability and rapid clearance.

In the pursuit of selective non-peptide TACE inhibitors much work has been done on the structure-based design of sulfonamide hydroxamates. The original series of sulfonamide hydroxamate inhibitors were based on an anthanilic acid scaffold [1], with the

* Corresponding author. Tel.: +1 512 448 8467; fax: +1 512 448 8492.
E-mail address: healy@stedwards.edu (E.F. Healy).

1093-3263/$ – see front matter © 2010 Elsevier Inc. All rights reserved.
doi:10.1016/j.jmgm.2010.08.006

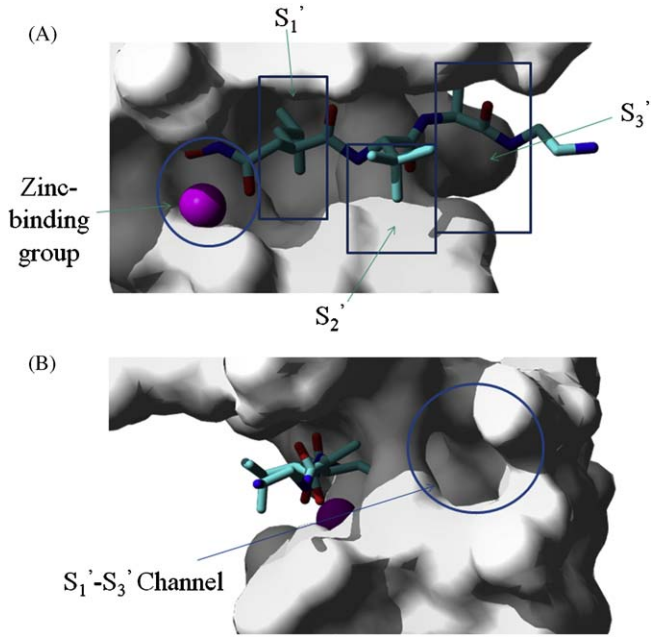

Fig. 1. Surface diagrams for the binding of TAPI-2 to TACE showing the ZBG, S_1'–S_3' active sub-sites (A) and the S_1'–S_3' channels (B).

anthranilate ring acting as a linker between the sulfonamide nitrogen and the hydroxamate, and a methoxyphenyl group attached to the sulfur and extending into to S_1' hydrophobic pocket. In an effort to mitigate the musculoskeletal side effects that normally plague the development of TACE inhibitors, enhanced selectivity over MMP-1, and to a lesser extent MMP-9 and MMP-13, was achieved by replacing the methoxy substituent on the P_1' group with a butynyloxy group. The prediction that the unique orientation of the channel connecting the S_1' and S_3' sub-sites in TACE, shown in Fig. 1B, would facilitate the insertion of the linear acetylenic group was borne out by the excellent in vitro potency observed for these inhibitors [2]. Inferring that the lack of sequence homology made it unlikely that the MMPs would have a similar S_1'–S_3' channel orientation the researchers predicted that this enhanced potency would be matched by increased selectivity. This indeed is what was observed. Shortening the spacer linkage between the sulfonamide nitrogen and the hydroxamate ZBG to a single sp^3 hybridized carbon yielded the potent inhibitor shown in Fig. 2B [3]. Ring closure between the nitrogen and this spacer carbon yielded the highly potent cyclic sulfonamide shown in Fig. 2C, otherwise known as TMI-1 [4]. Whereas fixing the sulfonyl group axial to the nitrogen had the expected result of ensuring a better fit of the P_1' substituent into the S_1' and S_3' channel, as witnessed by the increased potency of TMI-1, efforts at enhancing the potency further by facilitating hydrogen-bonding interactions between the butynyloxy terminus and residues in the S_3' pocket were not successful, as witnessed by the increase in IC_{50} values observed for inhibitor 2D as compared to TMI-1 [5]. Finally the extension of this scaffold to include substituents capable of binding in the non-primed sub-sites associated with the other side of the substrate scissile bond, such as the structure shown in Fig. 2E, has led to some of the most potent TACE inhibitors yet synthesized [6]. While the pharmacokinetic limitations of the hydroxamate group have led to newer generation inhibitors based on a variety of non-hydroxamate ZBGs [7] the structure–activity results available for inhibitors 2A–2E represent a wealth of data capable of yielding new and important insights.

While sharing only a 39% sequence identity phylogenetic profiling clearly identifies ADAM10 and ADAM17 as comprising a distinct and separate subfamily from the other ADAM proteins [8]. Both proteinases function by cleaving their substrates at an extracellular site proximal to the cell membrane, thereby releasing the soluble fragment from the cell surface. A recent review has identified at least fourteen substrates, implicated in a range of ADAM-mediated shedding events in CNS, inflammation and cancer, that can be cleaved by both ADAM10 and ADAM17 [9]. In these events one of the enzymes is normally associated with a constitutive shedding event while the other ADAM mediates induced cleavage. While a few ADAM10-specific inhibitors have been synthesized [10], the rational design of such targets has been complicated by the lack of a crystal structure for an ADAM10 catalytic domain. While a great deal is known regarding those elements of structure-based design important for the development of either MMP or TACE-specific inhibitors, a comparable understanding for TACE *vis-à-vis* ADAM10 has yet to be achieved.

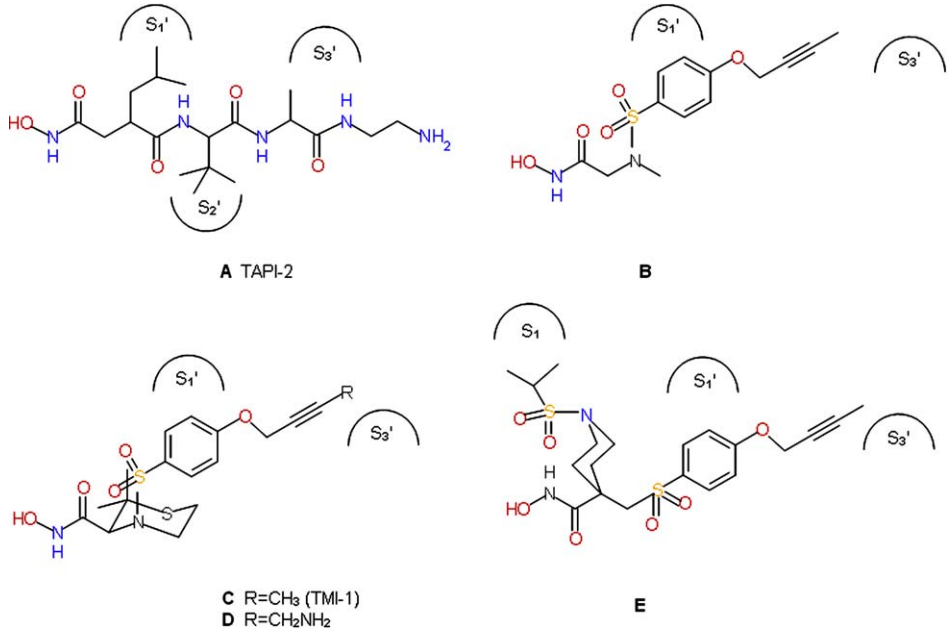

Fig. 2. Structures for the inhibitors modeled in this study.

This molecular modeling study seeks to build on this extensive body of structural activity data to better understand the structural nuances involved in the development of ever more potent TACE inhibitors. We also seek to identify those elements of structure-based design that enhance the selectivity of the inhibitor for TACE over ADAM10.

2. Methodology

2.1. Proteins

Crystal structures for the catalytic domain of ADAM17 bound to ligands 2A, 2C and 2D are available from the RCSB (www.rcsb.org) as PDB entries 1BKC [11], 1ZXC [4] and 2A8H [5] respectively. In addition PDB entry 2I47 [6], where the bound ligand contains a substituted isoxazole ring at the S_2 TACE sub-site, provides a suitable protein conformation for the docking of 2E. Finally, the protein conformation in 1ZXC also proved suitable for the docking of the sulfonamide 2B. After adding hydrogens, all proteins were subjected to a short energy minimization using the CHARMm force field [12], and successive steepest descent and conjugate gradient minimizations as implemented in the Discovery Studio program suite from Accelrys Inc. Although no crystal structure has yet been determined for the catalytic domain of ADAM10, a structure has been generated by homology modeling and is available from RCSB as PDB entry 1M1I [13]. This model was refined using molecular dynamics simulations in explicit solvent of complexes of the enzyme with *in vitro*-based substrates. The model that demonstrated greatest core stability and the most stable secondary structure was judged most plausible.

Proteins were aligned using the MODELER protocol as implemented in the Discovery Studio program suite.

2.2. $\Delta G_{binding}$

All ligands were docked to ADAM17 using CDOCKER [14], a docking algorithm based on the CHARMm force field that keeps the protein rigid but treats the ligand as fully flexible. Poses were refined in a final minimization step and ranked using a consensus scoring scheme that utilized two empirical scoring functions, LigScore1 and LigScore2 [15], two knowledge-based functions, PMF [16] and PMF04 [17], and the CDOCKER [14] CharmM-based energetic function. Comparison of the top-ranked result with experimental structures, where available, reproduced the X-ray finding with a root-mean-square deviation (rmsd) of less than 1.5 Å. For each ligand the docked complex was subjected to successive minimizations using steepest descent and Newton–Rhapson (NR).

In the absence of a ligand-bound complex a shape-directed docking methodology was employed to identify potential binding sites for ADAM10 with the TAPI-2 and TMI-1 ligands. The LigandFit protocol [18], as implemented in the Discovery Studio program suite, combines a cavity detection algorithm with a Monte Carlo-based conformational search to generate ligand poses consistent with the active site shape. Again the poses were ranked using a consensus scoring scheme and the highest ranked solution selected. The complex was then immersed in a truncated orthorhombic cell of TIP3P explicit water molecules, employing periodic boundary conditions, with the water molecules extending 7 Å from the surface of the protein and Na^+ and Cl^- ions added to neutralize the system. The system was minimized by steepest descent and conjugate gradient and then heated to 300 K. Equilibration was performed for 1 ns. The SHAKE algorithm was employed to keep bonds involving hydrogen atoms at their equilibrium length, allowing the use of a 2 fs time step. The equilibrated complex was finally subjected to successive steepest descent and NR minimizations.

Table 1
Experimental and calculated values of K_i, in units of nmol L^{-1}, for the binding of inhibitors 2A–2E with both TACE and ADAM10.

Protein		2A	2B	2C	2D	2E
TACE	K_i^{expt} (nM)	120	10	0.08		
	K_i^{calc} (nM)	120	19	0.10	0.15	1.4
ADAM10	K_i^{expt} (nM)	3000		16		
	K_i^{calc} (nM)	6720		26		

The estimation of the free energy of binding of all the non-covalent complexes is based on the assumption that $\Delta G_{binding} = G_{complex} - G_{protein} - G_{ligand}$, where G_X stands for the free energy of species X in aqueous solution at the standard concentration. G_X is further decomposed into the solute gas phase energy, solvation free energy $G_{solvation}$, and the solute entropy contributions, i.e., $G_X = E_{gas} + G_{solvation} - TS_{solute}$. E_{gas} is derived directly from energy calculations in vacuum. $G_{solvation}$ is decomposed into polar and nonpolar terms, i.e., $G_{solvation} = G_{polar} + G_{nonpolar}$ where G_{polar} is computed by continuum electrostatics, and $G_{nonpolar}$ is estimated based on the solvent accessible surface area of the solute. For this calculation the Generalized Born with simple SWitching (GBSW) [19] implicit solvent model, as implemented in the Discovery Studio program suite, was used. For ADAM10 complexes the explicit water molecules and the salt ions were removed prior to calculation of $\Delta G_{binding}$.

2.3. Molecular dynamics

In addition to the equilibration of docked complexes for ADAM10, molecular dynamic (MD) simulations were also performed on the top-ranked docked poses of ADAM17 complexed with ligands 2C and 2D. In both cases the initial complex was solvated with TIP3P explicit water molecules, occupying a sphere of

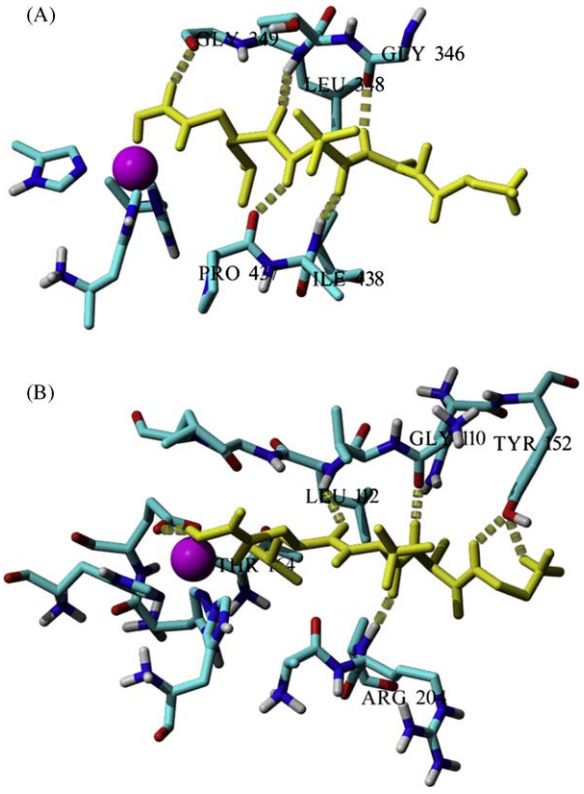

Fig. 3. Hydrogen-bonding interactions for the docked complex of TAPI-2 with TACE (A) and ADAM10 (B).

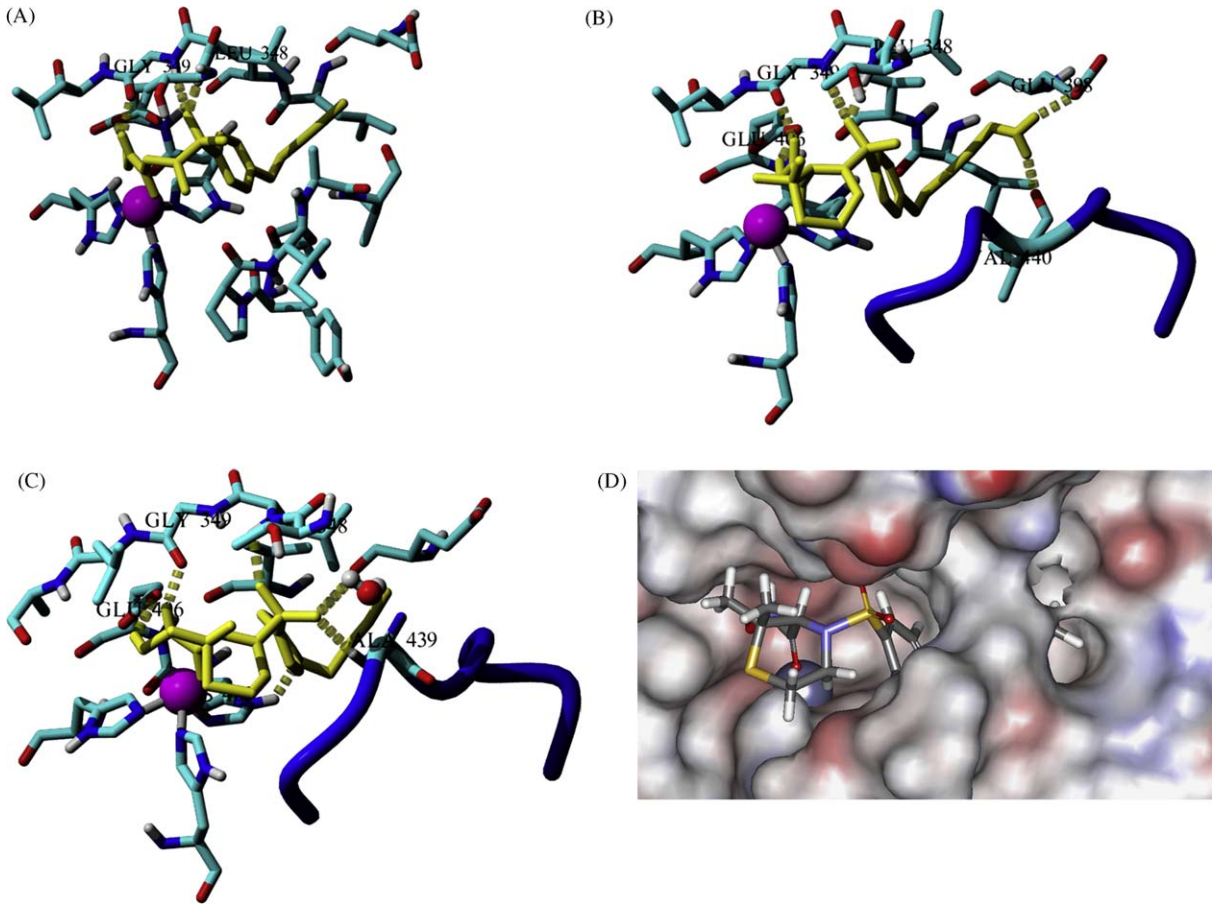

Fig. 4. Hydrogen-bonding interactions for the complex of TACE with inhibitor 2B (A); hydrogen-bonding interactions for the complex of TACE with inhibitor 2D, showing the position of the Tyr_{346} to His_{444} flexible loop (B); hydrogen-bonding interactions for the complex of TACE with TMI-1, optimized after solvation and a 1 ns equilibration, showing the position of the Tyr_{346} to His_{444} flexible loop and the position of a key water molecule, shown in ball and stick (C); solvent accessible structure (probe radius of 1.2 Å) for the TMI-1:TACE complex (D).

radius 15 Å from the surface of the bound ligand, and employing an explicit spherical boundary with harmonic restraint. The system was minimized by steepest descent and conjugate gradient and then heated to 300 K. After equilibration for 1 ns production runs of 1 ns duration were obtained. The SHAKE algorithm was employed to keep bonds involving hydrogen atoms at their equilibrium length, allowing the use of a 2 fs time step.

3. Results and discussion

3.1. Potency

Experimental K_i values have been reported for the binding of inhibitors 2A–2C to TACE. While no experimental binding constants are available for inhibitors 2D and 2E IC_{50} values identify these inhibitors as being approximately 8 times less effective [5], and 6 times more effective [6], respectively, relative to inhibition by TMI-1. Experimental and calculated K_i values for the inhibition of TACE by inhibitors 2A–2E are reported in Table 1.

From Fig. 3A we can see that in addition to its occupancy of the S_1'–S_3' binding sub-sites and the zinc-binding efficiency of the hydroxamate group, the nanomolar effectiveness of TAPI-2 inhibition of TACE can also be attributed to the extensive hydrogen bonding between the peptidomimetic backbone and five active site residues. The order of magnitude increase in binding effectiveness for sulfonamide 2B, Fig. 4A, partly reflects the benefit of more effective binding of the aryl system within the S_1' hydrophobic pocket as well the extension of the butynyloxy group into the S_1'–S_3' channel. The presence of the sulfonyl oxygens also aids in maintaining two of the inhibitor-TACE hydrogen bonds, most critically the hydrogen bond to the amide hydrogen of Leu_{348}, which helps extend and fix the aromatic ring within the S_1' cleft.

The decrease in K_i by a further two orders of magnitude for inhibitors 2C and 2D reflects the enhanced binding affinity achieved by cyclizing the sulfonamide nitrogen and the spacer carbon in a thiomorpholine ring system. However the near equal $\Delta G_{binding}$ values calculated for these two ligand stands in marked contrast to the experimental observation that, despite the existence of two additional hydrogen bonds between the acetylenic amino group and the side chain of Glu_{398} and the backbone of Ala_{440}, inhibitor 2D is over 8 times less effective than TMI-1, as measured by the experimental IC_{50} values [5]. A molecular dynamics simulation of partially solvated complexes of 2C and 2D with TACE provides an unexpected explanation for the greater binding effectiveness of TMI-1. Whereas equilibration of a solvated complex of 2D with TACE yields a structure essentially equivalent to that provided by the crystal structure, a 1 ns equilibration of partially solvated TMI-1 results in a small, but significant, conformational shift of a loop connecting residues Tyr_{346} and His_{444}, Fig. 4C. This repositioning allows for the formation of another hydrogen bond, this time between the second sulfonyl oxygen and the amide hydrogen of Ala_{439}. Additionally, and potentially of greater importance, is the fact that movement of this loop allows for the more effective exclusion of solvent from the region of the bound ligand, specifically from the S_1'–S_3' channel, as shown in Fig. 4D. The structural

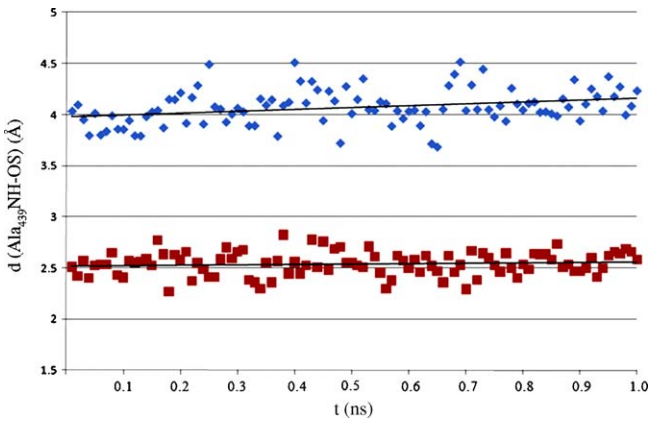

Fig. 5. Trajectory analysis for the SO–HN(Ala_{439}) distance, for a 1 ns MD simulation, TACE bound to TMI-1 (square) and TACE complexed with inhibitor 2D (diamond).

advantage of such solvent exclusion can be seen by analyzing the trajectory of this newly formed SO–HN(Ala_{439}) hydrogen bond over a MD production run for TMI-1 bound to TACE, compared to the trajectory of the same interaction for inhibitor 2D, Fig. 5. The persistence of the hydrogen-bonding interaction observed for TMI-1 over the 1 ns timescale is in marked contrast to the wide variability observed for the much longer SO–HN(Ala_{439}) distance found in the complex for inhibitor 2D. This greater movement undoubtedly co-relates with less efficient binding, and explains the larger IC_{50} values observed experimentally. That conformational change leading to solvent exclusion can lead to more effective hydrogen bonding, and thus more effective ligand binding, has been previously proposed by us [20] and others [21]. This inherent flexibility in the unstructured loop spanning Tyr_{436} to His_{444} is evidenced by differing values of 4.5 Å and 4.9 Å for the distance between the sulfonyl oxygen and the Ala_{439} nitrogen observed for the two subunits of PDB entry 1BKC. This difference corresponds to a variation of almost 0.5 Å for the (ligand) SO–HN(Ala_{439}) when modeled as the CHARMm-minimized structure, and highlights the inherent flexibility of the Tyr_{436}–His_{444} loop.

A similarly flexible loop, ranging in length from eight to eleven residues and of no particular secondary structure, has been identified for a wide range of MMPs [22]. Comparison of uninhibited MMP-3 with an inhibitor bound complex reveals a substantial conformational change involving movement of this loop, and caused by an inhibitor-induced displacement of Tyr_{223} [23]. This tyrosine residue corresponds to Ala_{439} in TACE and is found consistently throughout a wide range of MMPs, e.g. as Tyr_{423} in MMP-9 [24]. The flexibility of this tyrosine-containing loop has also been observed in solution structures of MMPs determined by NMR [25], and has been simulated by MD [26].

The inhibitor 2E contains a sterically bulky sulfonamide isopropyl group designed to bind to the S_1 sub-site. This α-piperidine β-sulfone scaffold design was found to increase the potency against TACE, and broaden the selectivity over a wider range of MMPs [6]. In addition introducing a steric block alpha to the hydroxamate group is known to suppress metabolism of the labile ZBG, thus potentially increasing the *in vivo* potency [27]. While our calculated $\Delta G_{binding}$ for 2E was approximately 1.5 kcal mol^{-1} higher than that calculated for TMI-1, as opposed to the observed six-fold decrease in the IC_{50}, the complex formed clearly shows the binding of the isopropyl group in the predominantly hydrophobic S_1 cleft, Fig. 6A. Of greater interest to us here is the binding pocket distal to S_1, a cleft presumably representing the S_2 sub-site. Whereas a previous characterization identified this S_2 pocket as comprising residues His_{409} to His_{415} inclusive [28], inspection of Fig. 6A identifies the cleft as mainly defined by His_{409}, Glu_{414} and His_{415},

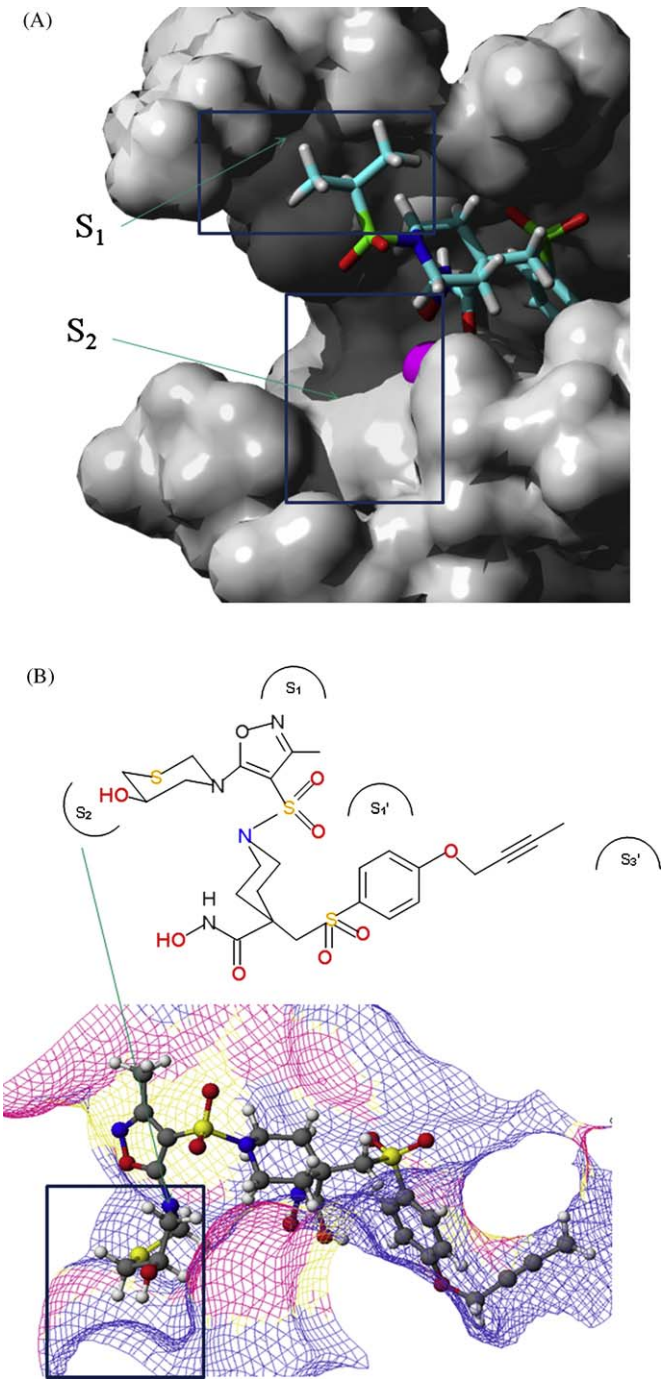

Fig. 6. Surface diagram showing the complexation of inhibitor 2E with TACE (A); structure for putative picomolar inhibitor of TACE showing an electrostatic map of the active site surrounding this ligand (B).

with some definition also added by Val_{353}. A modification of the ligand that demonstrated the greatest potency and highest selectivity against MMPs, 5E with a 3,-5 dimethyl isoxazole instead of the isopropyl group as the P_1 substituent, is shown in Fig. 6B. By attaching a hydroxy-substituted thiomorpholine ring in place of one of the methyl groups one can extend the scaffold to a structure with a P_2 substituent. A successful dock of this putative inhibitor yielded a calculated K_i of approximately 1 pM. The electrostatic map of the active site surrounding this ligand is also shown in Fig. 6B, with a cream color indicating that the ligand should have a hydrophobic surface at that position to achieve good binding, a red color marks a site on the ligand that would benefit from hydrogen-bond

acceptors, and blue marking a ligand design that would benefit from hydrogen-bonding donors. Fig. 6B indicates that while the hypothetical substituent sits perfectly in the cleft further modification would most likely yield an inhibitor with an even lower calculated K_i.

3.2. Selectivity

Experimental K_i values have also been determined for the binding of TAPI-2 and TMI-1 to ADAM10, and these, along with values calculated in this study, are reported in Table 1. Cursory analysis of the binding of TAPI-2 to ADAM10, Fig. 3B, identifies the same number of ligand protein hydrogen bonds as found in the TACE complex. However analysis of a short 0.5 ns MD production run showed that the hydrogen bonds between the terminus of the diaminoethyl P'_3 substituent and the tyrosine residue readily break and reform. This lack of persistence is caused both by solvation and rotation of the C–N and C–C bonds in the diaminoethyl group. This result is to be expected given the exposed nature of this portion of the active site, and undoubtedly signifies that these two hydrogen bonds should be substantially less effective than those between the TAPI-2 backbone and the other residues. This is reflected in a much weaker, both calculated and observed, micromolar inhibition of ADAM10 by TAPI-2.

While inhibitor 2E exhibits much greater selectivity for TACE over MMP-1 and MMP-9, and to a lesser but still significant extent over MMP-2 and MMP-13, TMI-1 displays markedly less selectivity for TACE over MMP-1 and MMP-9, and no selectivity at all over MMP-13 [6]. Surprisingly, given their similar phylogenetic profile [8], TMI-1 remains moderately selective for TACE over ADAM10, as shown by the values for K_i in Table 1. A close inspection of the geometry surrounding the bound ligand in both TACE and ADAM10 provides a possible clue as to why this is the case. Identifying three apices as the zinc-metal center, the nitrogen hydrogen-bonding donor of Leu_{348} and the nitrogen hydrogen-bonding donor of Ala_{439}, one obtains a triangle with sides of 8.4 Å, 7.1 Å and 7.6 Å that describes the fit of the ligand within the active site of TACE, Fig. 7B. A similar triangular fit to ADAM10 yields far different lengths of 8.5 Å, 8.8 Å and 10.9 Å, the latter length defining the distance of the "base" from the zinc to the nitrogen of Ala_{439}, Fig. 7A. This would indicate that while TMI-1 is capable of utilizing the hydroxamate group to bind to the zinc while at the same time extending the butynyloxy group into the S_1'–S_3' channel in TACE, the size of the active site prevents both interactions from being simultaneously realized in ADAM10. The minimized structure giving the K_i value reported in Table 1 shows preferential insertion of the acetylenic group into the S_1'–S_3' channel that leaves the complex with (hydroxamate) O–Zn distances of 3.6 Å and 4.6 Å, substantially longer that the corresponding distances of 3.0 Å and 2.2 Å found in TACE. The over two-fold increase in the carbonyl oxygen to metal distance presumably contributes most to the lower potency for inhibition of ADAM10 by TMI-1.

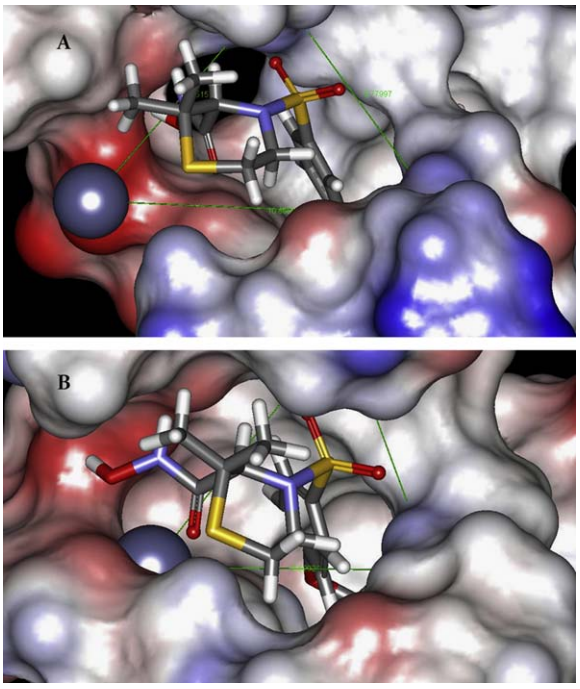

Fig. 7. Geometry of TMI-1 complex, defining a triangle from the zinc-metal center to the nitrogen hydrogen-bonding donor of Leu_{348} and on to the nitrogen hydrogen-bonding donor of Ala_{439}, with distances of 8.5 Å, 8.8 Å and 10.9 Å for ADAM10 (A), and of 8.4 Å, 7.1 Å and 7.6 Å for TACE (B).

Alignment, using the MODELER protocol as implemented in the Discovery Studio program suite, of TACE complexed with the newly designed inhibitor shown in Fig. 6B and ADAM10 complexed with TAPI-2 gives the active sub-site assignments for ADAM10 shown in Fig. 8. While much of the sub-site composition is shared among the two enzymes, some key differences may provide a guide in the future design of inhibitors for greater selectivity over either TACE or ADAM10. Specifically the substitution of a proline in ADAM10 for the Glu_{414} in TACE within the S_2 sub-site should allow for the incorporation of P_2 substituents capable of discriminating between the constitutive and induced shedding events mediated by these enzymes.

In analyzing these results one needs to remain mindful of the fact that the crystal structures available for TACE are just those of the catalytic, or metalloproteinase, domain, and that the homology modeled structure for the similar domain in ADAM10 is just that—a modeled structure. ADAM structures are also comprised of transmembrane domains, disintegrin and cysteine-rich domains, and possibly most importantly prodomains. These latter prodomains have been well characterized [29] as possessing an autoinhibitory capability, and interestingly the prodomain of ADAM10 inhibits TACE with the same potency as its own prodomain though sharing only a 29% sequence identity at their prodomains. Additionally,

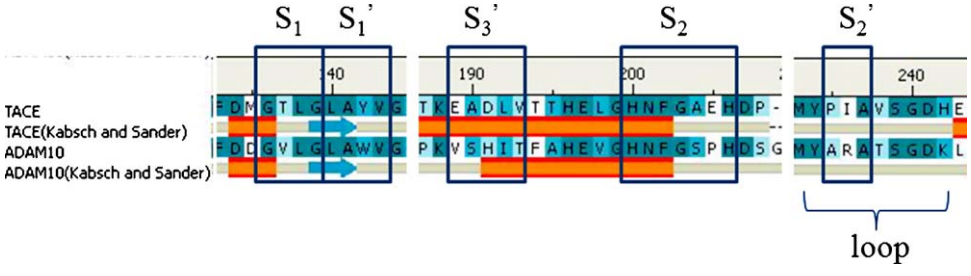

Fig. 8. Alignment of TACE and ADAM10 showing the active sub-site assignments for ADAM10 and predicted elements of secondary structure.

these prodomains are thought to operate as essentially intramolecular chaperones as they aid in the secretion of the activated enzyme. This complexity, in both structure and function, means that modeling of the catalytic domain, though explanatory and potentially predictive, represents only a portion of what is required in order to achieve a complete understanding of the physiological activity of these systems.

Acknowledgements

The authors are grateful to the W.M. Keck Foundation and the Educational Advancement Foundation (EAF) for their generous support of this work. We also wish to acknowledge the support of the National Science Foundation (Grant # DUE-0969153), and thank the Welch Foundation (Grant # BH-0018) for its continuing support of the Chemistry Department at St. Edward's University.

References

[1] J.I. Levin, M.T. Du, J.F. DiJoseph, L.M. Killar, A. Sung, T. Walter, M.A. Sharr, C.E. Roth, F.J. Moy, R. Powers, G. Jin, R. Cowling, J.S. Skotnicki, The discovery of anthranilic acid-based MMP inhibitors. Part 1: SAR of the 3-position, Bioorg. Med. Chem. Lett. 11 (2001) 235–238.
[2] J.M. Chen, G. Jin, A. Sung, J.I. Levin, Anthranilate sulfonamide hydroxamate TACE inhibitors. Part 1: Structure-based design of novel acetylenic P1′ groups, Bioorg. Med. Chem. Lett. 12 (2002) 1195–1198.
[3] J.I. Levin, J.M. Chen, K. Cheung, D. Cole, C. Crago, E.D. Santos, X. Du, G. Khafizova, G. MacEwan, C. Niu, E.J. Salaski, A. Zask, T. Cummons, A. Sung, J. Xu, Y. Zhang, W. Xu, S. Ayral-Kaloustian, G. Jin, R. Cowling, D. Barone, K.M. Mohler, R.A. Black, J.S. Skotnicki, Acetylenic TACE inhibitors. Part 1. SAR of the acyclic sulfonamide hydroxamates, Bioorg. Med. Chem. Lett. 13 (2003) 2799–2803.
[4] J.I. Levin, J.M. Chen, L.M. Laakso, M. Du, X. Du, A.M. Venkatesan, V. Sandanayaka, A. Zask, J. Xu, W. Xu, Y. Zhang, J.S. Skotnicki, Acetylenic TACE inhibitors. Part 2: SAR of six-membered cyclic sulfonamide hydroxamates, Bioorg. Med. Chem. Lett. 15 (2005) 4345–4349.
[5] J.I. Levin, J.M. Chen, L.M. Laakso, M. Du, J. Schmid, W. Xu, T. Cummons, J. Xu, G. Jin, D. Barone, J.S. Skotnicki, Acetylenic TACE inhibitors. Part 3: Thiomorpholine sulfonamide hydroxamates, Bioorg. Med. Chem. Lett. 16 (2006) 1605–1609.
[6] J.S. Condon, D. Joseph-McCarthy, J.I. Levin, H.G. Lombart, F.E. Lovering, L. Sun, W. Wang, W. Xu, Y. Zhang, Identification of potent and selective TACE inhibitors via the S1 pocket, Bioorg. Med. Chem. Lett. 17 (2007) 34–39.
[7] S. DasGupta, P.R. Murumkar, R. Giridhar, M.R. Yadav, Current perspective of TACE inhibitors: a review, Bioorg. Med. Chem. 17 (2009) 444–459.
[8] C. Antczak, C. Radu, H. Djaballah, A profiling platform for the identification of selective metalloprotease inhibitors, J. Biomol. Screen. 13 (2008) 285–294.
[9] J. Pruessmeyer, A. Ludwig, The good, the bad and the ugly substrates for ADAM10 and ADAM17 in brain pathology, inflammation and cancer, Semin. Cell Dev. Biol. 20 (2009) 164–174.
[10] A. Ludwig, C. Hundhausen, M.H. Lambert, N. Broadway, R.C. Andrews, D.M. Bickett, M.A. Leesnitzer, J.D. Becherer, Metalloproteinase inhibitors for the disintegrin-like metalloproteinases ADAM10 and ADAM17 that differentially block constitutive and phorbol ester-inducible shedding of cell surface molecules, Comb. Chem. High Throughput Screen. 8 (2005) 161–171.
[11] K. Maskos, C. Fernandez-Catalan, R. Huber, G.P. Bourenkov, H. Bartunik, G.A. Ellestad, P. Reddy, M.F. Wolfson, C.T. Rauch, B.J. Castner, R. Davis, H.R. Clarke, M. Petersen, J.N. Fitzner, D.P. Cerretti, C.J. March, R.J. Paxton, R.A. Black, W. Bode, Crystal structure of the catalytic domain of human tumor necrosis factor-alpha-converting enzyme, Proc. Natl. Acad. Sci. U.S.A. 95 (1998) 3408–3412.
[12] B.R. Brooks, R.E. Bruccoleri, B.D. Olafson, D.J. States, S. Swaminathan, M. Karplus, CHARMM: a program for macromolecular energy, minimization, and dynamics calculations, J. Comput. Chem. 4 (1983) 187–217.
[13] A. Herington, S. Manzetti, D. Mcculloch, D. van der Spoel, Modeling of Enzyme-Substrate Complexes for the Metalloproteases MMP-3, ADAM-9 and ADAM-10, J. Comput. Aided Mol. Des. 17 (2003) 551–565.
[14] G. Wu, D.H. Robertson, C.L. Brooks III, M. Vieth, Detailed analysis of grid-based molecular docking: a case study of CDOCKER – A CHARMm-based MD docking algorithm, J. Comput. Chem. 24 (2003) 1549–1562.
[15] A. Krammer, P.D. Kirchhoff, X. Jiang, C.M. Venkatachalam, M. Waldman, LigScore: a novel scoring function for predicting binding affinities, J. Mol. Graph. Model. 23 (2005) 395–407.
[16] I. Muegge, Y.C. Martin, A general and fast scoring function for protein–ligand interactions: a simplified potential approach, J. Med. Chem. 42 (1999) 791–804.
[17] I. Muegge, PMF scoring revisited, J. Med. Chem. 49 (2006) 5895–5902.
[18] C.M. Venkatachalam, X. Jiang, T. Oldfield, Waldman M, LigandFit: a novel method for the shape-directed rapid docking of ligands to protein active sites, J. Mol. Graph. Model. 21 (2003) 289–307.
[19] W. Im, M.S. Lee, C.L. Brooks, Generalized born model with a simple smoothing function, J. Comput. Chem. 24 (2003) 1691–1702.
[20] E.F. Healy, S. Johnson, C. Hauser, P. King, Tyrosine kinase inhibition: ligand binding and conformational change in c-Kit and c-Abl, FEBS Lett. 583 (2009) 2899–2906.
[21] A. Fernández, R. Scott, Dehydron: a structurally encoded signal for protein interaction, Biophys. J. 85 (2003) 1914–1928.
[22] B.G. Rao, Recent developments in the design of specific matrix metalloproteinase inhibitors aided by structural and computational studies, Curr. Pharm. Des. 11 (2005) 295–322.
[23] L. Chen, T.J. Rydel, F. Gu, C.M. Dunaway, S. Pikul, K.M. Dunham, B.L. Barnett, Crystal structure of the stromelysin catalytic domain at 2.0 A resolution: inhibitor-induced conformational changes, J. Mol. Biol. 293 (Oct 1999) 545–557.
[24] B.G. Rao, U.K. Bandarage, T. Wang, J.H. Come, E. Perola, Y. Wei, S.K. Tian, J.O. Saunders, Novel thiol-based TACE inhibitors: rational design, synthesis, and SAR of thiol-containing aryl sulfonamides, Bioorg. Med. Chem. Lett. 17 (2007) 2250–2253.
[25] P.R. Gooley, J.F. O'Connell, A.I. Marcy, G.C. Cuca, M.G. Axel, C.G. Caldwell, W.K. Hagmann, J.W. Becker, Comparison of the structure of human recombinant short form stromelysin by multidimensional heteronuclear NMR and X-ray crystallography, J. Biomol. NMR 7 (1996) 8–28.
[26] M. Aschi, D. Roccatano, A. Di Nola, C. Gallina, E. Gavuzzo, G. Pochetti, M. Pieper, H. Tschesche, F. Mazza, Computational study of the catalytic domain of human neutrophil collagenase. specific role of the S_3 and S_3' subsites in the interaction with a phosphonate inhibitor, J. Comput. Aided Mol. Des. 16 (2002) 213–225.
[27] J.F. Fisher, S. Mobashery, Recent advances in MMP inhibitor design, Cancer Metastasis Rev. 1 (2006) 115–136.
[28] V. Lukacova, Y. Zhang, D.M. Kroll, S. Raha, D. Comez, S. Balaz, A comparison of the binding sites of matrix metalloproteinases and tumor necrosis factor-alpha converting enzyme: implications for selectivity, J. Med. Chem. 48 (2005) 2361–2370.
[29] P.E. Gonzales, J.D. Galli, M.E. Milla, Identification of key sequence determinants for the inhibitory function of the prodomain of TACE, Biochemistry 47 (2008) 9911–9919.